JOURNAL OF MATERIALS SCIENCE 32 (1997) 6069–6073

Microcracks in chromium electrodeposits

N. M. MARTYAK, J. E. McCASKIE
Atotech USA, Inc., Somerset, NJ 08875, USA

B. VOOS, W. PLIETH
Technische Universitat Dresden, Institut fur Physikalische Chemie und Elektrochemie, Mommsenstraße 13, 01069 Dresden, Germany

The internal stress in chromium deposits plated using a sulphate catalyst was determined using a bent cathode method. Chromium deposits exhibited a high internal tensile stress which decreased with increasing deposit thickness. Surface structures and microcrack patterns were studied using secondary electron and *y*-modulation techniques and atomic force microscopy (AFM). *Y*-modulation images revealed some three-dimensional information about microcracks. AFM analysis provided quantitative information about microcrack widths and depths.

1. Introduction

There are two classes of internal stresses in electrodeposited coatings [1–4]: extrinsic stresses are due to the interaction between the deposit and the substrate, and intrinsic stresses develop independently of the substrate. Type I, frequently called macrostresses, extends over wide regions of the deposit without a change in sign. Type I stresses are either tensile or compressive and may cause bending of a metal strip. Type I tensile stresses develop in metals when layers near the surface of the deposit attempt to shrink after being deposited and the substrate material tries to prevent the volume decrease. Tensile stresses may also develop if the deposit is forced to fit on the crystal lattice of a substrate which has larger interatomic spacing. Reid [5] proposed that the internal stress in electrodeposited metals may develop as a result of base-metal effects, metals deposited in a metastable condition and alteration of the deposit structure by the incorporation of foreign atoms.

Types II and III stresses extend over microscopic regions of the material and exhibit a net value of zero over macroscopic regions. Type II stress is due to strains at crystallite boundaries. Type III stresses are due to local distortions in the crystallite lattice [6]. Both Types II and III stresses do not distort the deposit but rather manifest themselves in the hardness of the material [7].

The measurement of internal stress in electrodeposits has been reviewed by Weil [4], Gabe and West [8] and Adzhiev and Solov'eva [9]. The simplest means of measuring the internal macrostress is the bent or flexible cathode. One side of the cathode is insulated. As the deposited metal is in tension, the cathode tends to deflect towards the anode. There are several different ways to measure the degree of deflection. Stoney [10] correctly developed the equations relating the degree of deflection to the internal stress. Barklie and Davies [11] used optical devices to record the deflection of the cathode. There are disadvantages to the bent cathode method for stress measurements. The insulation used to insulate the back side of the cathode may contaminate the plating solution. The insulation also affects the rigidity of the strip thereby altering the deflection. The coating material may dissolve or partially come off during the plating process, so metal is deposited on the back side of the cathode. As the cathode deflects towards the anode, the current distribution on the cathode changes and affects the tensile stress. Baurmann *et al.* [12] believed that the tensile stress may be partially relieved during the deflection, thereby yielding values lower than the true ones.

This study was undertaken to study the microcrack pattern that develops as a result of tensile stresses in chromium deposits. Specifically, three-dimensional information about microcracks is presented from SEM *y*-modulation data and atomic force microscopy (AFM) images. Internal stress measurements were made using a modified bent cathode device (Deposit stress analyses, Electrochemical Company Inc, York, PA).

2. Experimental procedure

Chromium plating solutions were prepared by dissolving 1.0 M CrO_3 in 1 l water. Sulphuric acid, 0.05 M, was added after the chromium oxide completely dissolved. The chromium sulphate solution was operated at 40 °C and 500 mA cm^{-2}. After plating, the surface of the chromium layers was rinsed in distilled water and dried. Some of the samples were etched to develop the microcrack pattern. Etching of the surface was done by making the part anodic in 100 g/l NaOH at 50 °C. The sample was etched for 0.5 A min cm^{-2}. Unetched and etched samples were studied using SEM and AFM.

The internal stress was determined by a deposit stress analyser (Electrochemical Company, York, PA).

0022–2461

A stress test strip consisted of copper alloy strips insulated on one and opposite sides. The stress strips were weighed before and after plating and from the weight gain, the thickness of chromium was calculated. Plating of chromium was done on one side of a copper alloy strip and allowed to bend towards the anode. The degree of curvature was determined from a test-strip measuring block and the stress calculated.

3. Results and discussion

The internal stress in the chromium deposit plated from the sulphate electrolyte shows a tensile stress curve characteristic of hexavalent chromium deposits [13–15]. Fig. 1 shows the stress decreases from an initially high tensile stress to a lower limiting value. Previous studies [13] have shown the stress is initially high and due to the coalescence of three-dimensional crystallites. At a given thickness, dependent upon the nature of the substrate, the chromium deposit starts to crack owing to the high internal tensile stress. The method to measure stress in this study is not sensitive enough to determine the internal tensile stresses prior to crystallite coalescence. Because no maximum in tensile stress is seen in Fig. 1, crystallite coalescence is complete and microcracking within the chromium deposit has occurred to an appreciable extent.

SEM analysis of the chromium sulphate deposit reveals a network of microcracks approximately 0.05–0.1 μm across, Fig. 2. Large microcracks are seen as well as smaller, fainter cracks. Etching the chromium deposit in caustic soda develops the microcrack network as seen in Fig. 3. Etching appears to increase the size of the cracks which are now about 0.5 μm in size. The surface microcracks are dark but fainter microcracks are also seen in Fig. 3. These less well-developed cracks are below the surface and formed in the chromium deposit earlier during the deposition process. These subsurface microcracks are the open voids often seen in cross-sections of chromium deposits [16].

A secondary electron image of the same etched chromium deposit at $\times 2000$ is seen in Fig. 4. Large well-developed surface microcracks are seen with subsurface microcracks also apparent. Adjacent to the microcracks are bright areas. Using a secondary electron detector, brighter areas indicate either material is higher above neighbouring regions or material charging. Imaging the same area, a *y*-modulation mode

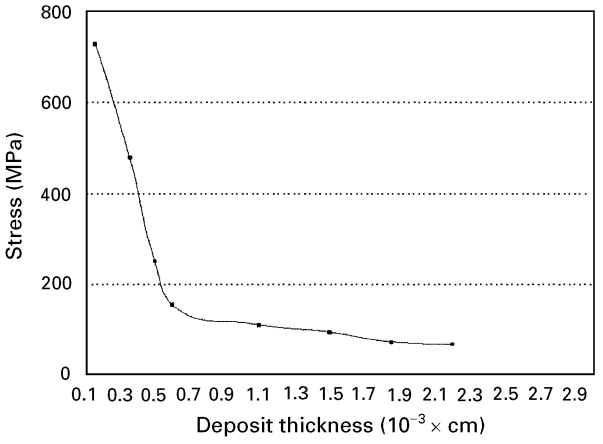

Figure 1 Stress curve showing decrease in tensile stress with deposit thickness. (■) CrO_3–SO_4.

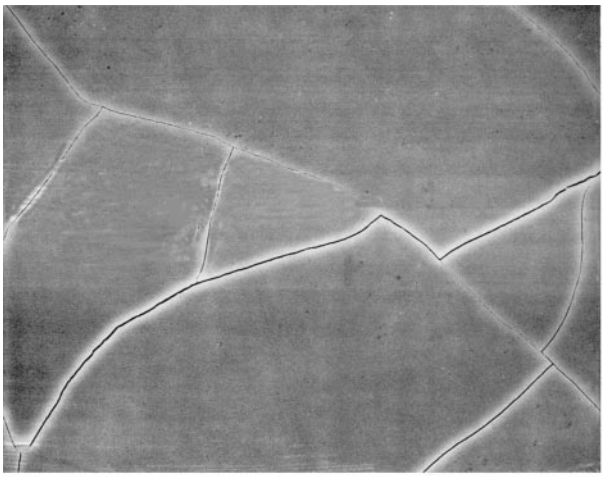

Figure 2 SEM image of chromium deposit, unetched ($\times 2000$).

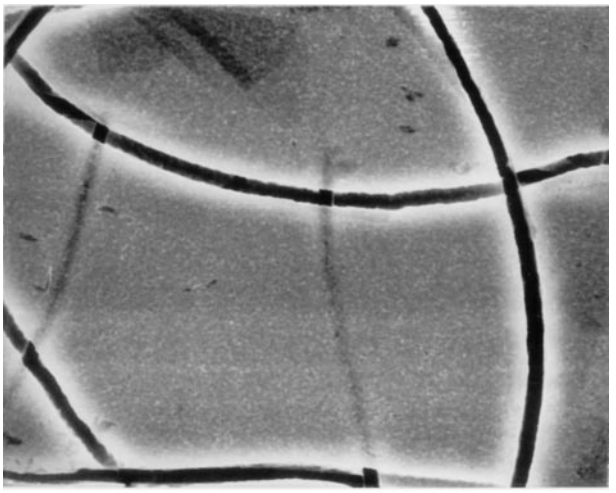

Figure 3 SEM image of etched chromium deposit showing microcracks ($\times 5000$).

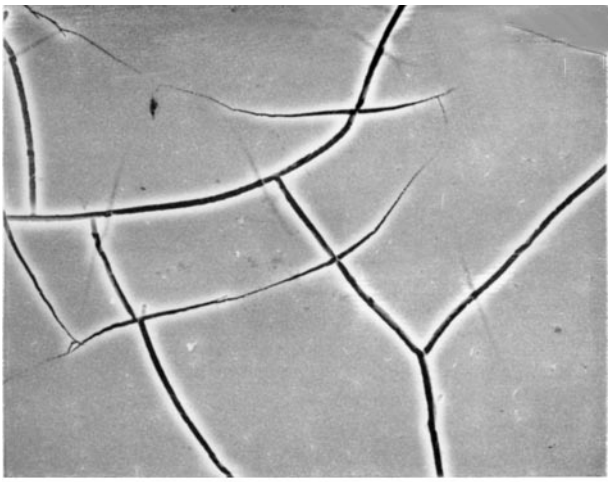

Figure 4 Secondary electron image of etched chromium deposit ($\times 2000$).

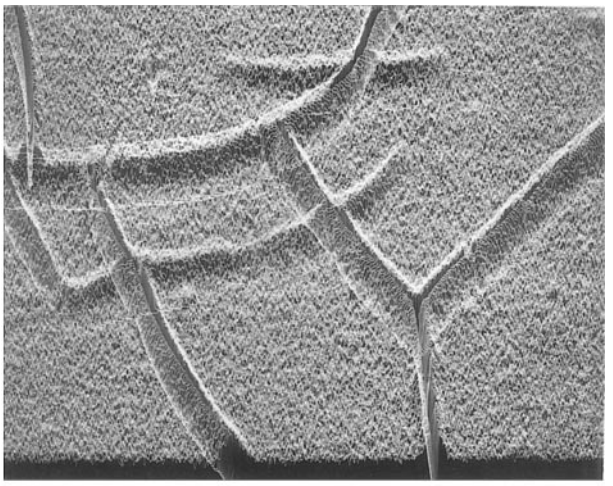

Figure 5 *Y*-modulation image of etched chromium deposit (× 2000).

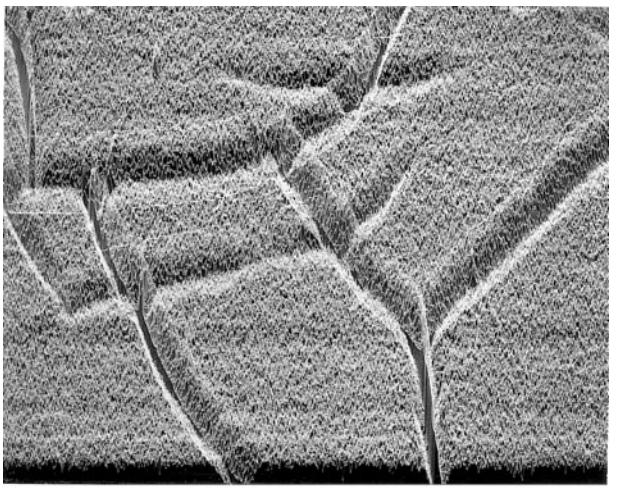

Figure 7 Inverted *Y*-modulation image of etched chromium deposit (× 2000).

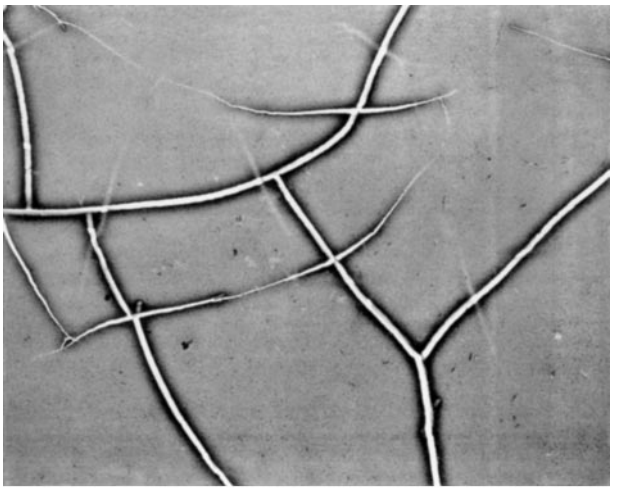

Figure 6 Inverted secondary electron image of etched chromium deposit (× 2000).

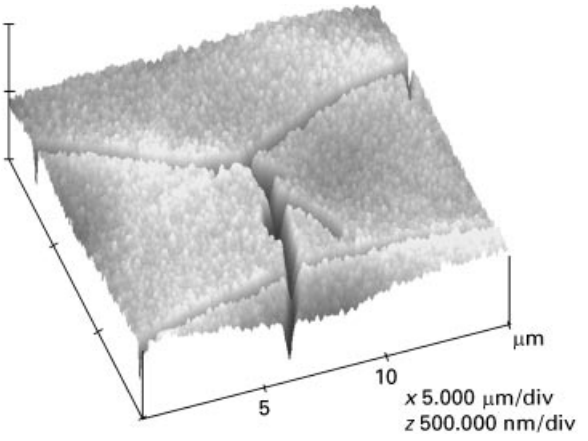

Figure 8 AFM surface plot of chromium deposit showing microcracks.

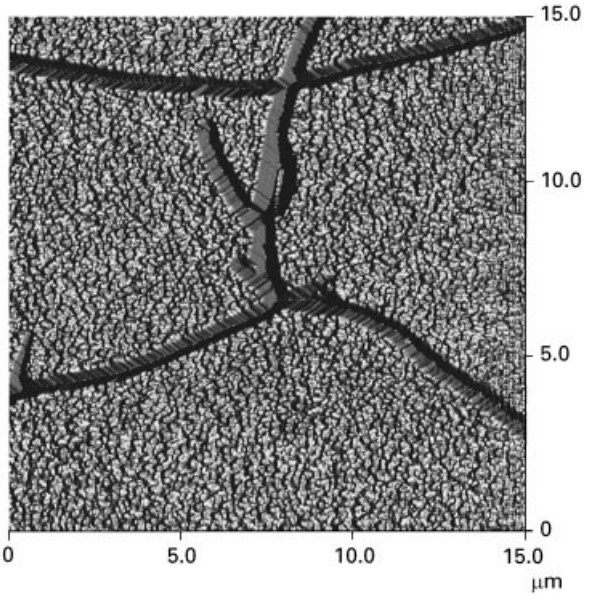

Figure 9 AFM top view showing microcracks in the chromium surface.

provides three-dimensional information, Fig. 5. The microcracks are seen as well as fine structure within the bulk of the deposit. The microcracks are seen as depressions throughout the coating whereas the chromium adjacent to the microcracks appears higher than that either in the bulk of the deposit or within the microcrack. This raised relief is the bright areas in Fig. 4. To confirm further the nature of the materials adjacent to the microcracks, the secondary electron image of Fig. 4 is inverted in Fig. 6. The microcracks are now higher than the remaining portions of the chromium coating, causing a larger fraction of secondary electrons to reach the detector and thus appear brighter. Note the area immediately adjacent to the microcracks is darker than the bulk chromium coating, indicating recessed areas. Similarly, a *y*-modulated image of the inverted image shown in Fig. 7 reveals the third dimension of the secondary electron image. The microcracks are seen to rise above the rest of the chromium deposit, whereas areas next to the inverted microcracks are lower than that of the bulk chromium deposit. Previous studies have shown that the material directly adjacent to the microcracks in chromium, as seen in Figs 4 and 6, is higher in sulphur compared to the bulk of the deposit [13]. It was postulated that microcracks propagate along these regions higher in sulphur as the sulphur acts as

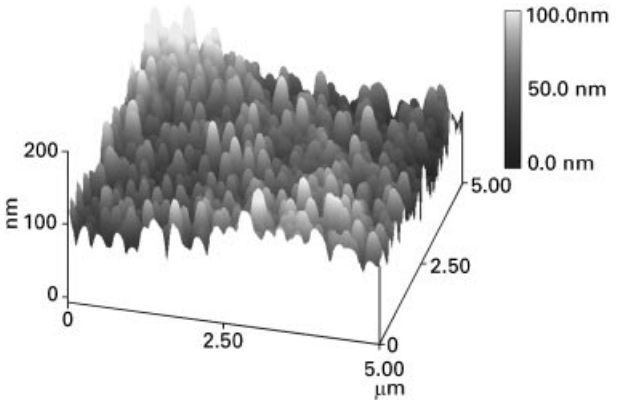

Figure 10 AFM surface plot of fine structure in the chromium coating.

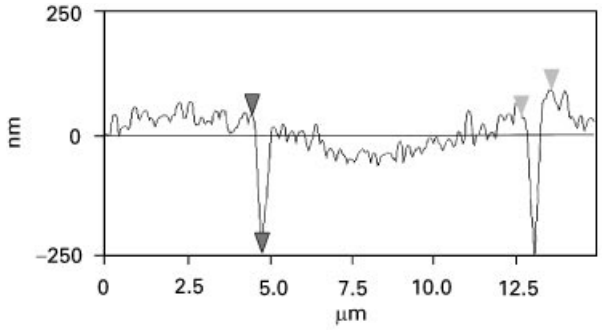

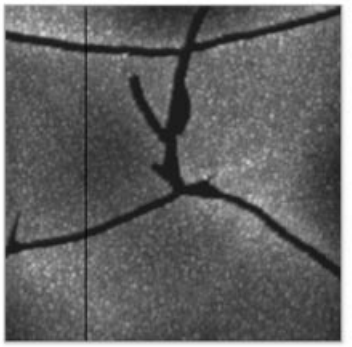

Figure 11 AFM sectional analysis detailing microcrack width and depth. Horizontal distance, *L*, 0.293 μm; vertical distance, 268.05 μm; Angle 42.457°. Horizontal distance 0.908 μm, vertical distance 24.951 μm, Angle 1.574°. Horizontal distance, vertical distance, Angle. Spectral period d.c., spectral frequency 0.000 Hz, spectral amplitude 2.785 nm.

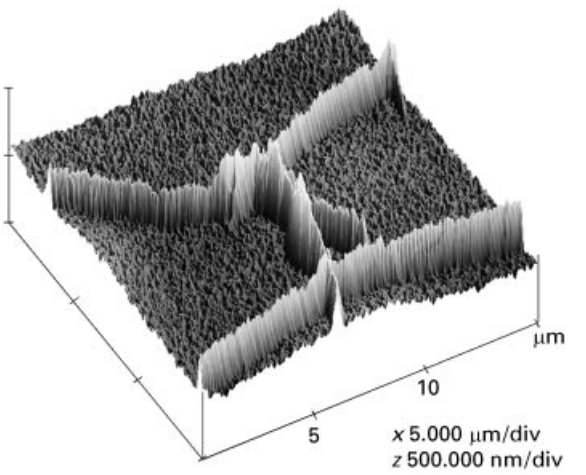

Figure 12 AFM inverted surface plot showing the structure of microcracks within the chromium coating.

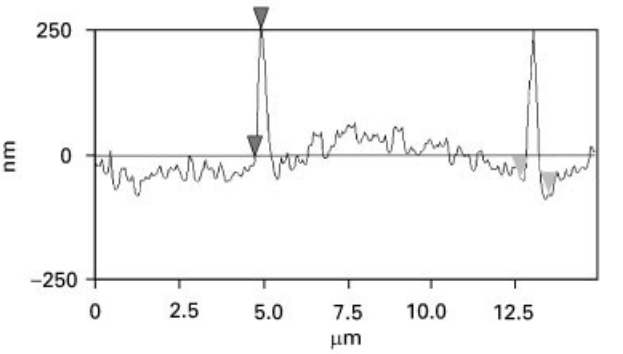

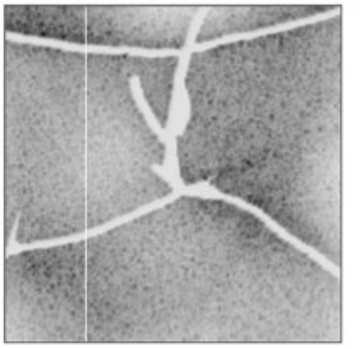

Figure 13 AFM sectional analysis of an inverted image detailing microcrack width and height. Horizontal distance, *L*, 0.264 μm; vertical distance, 267.88 μm; Angle 45.454°. Horizontal distance, 0.820 μm; vertical distance, 32.775 μm; Angle 2.288°. Horizontal distance, vertical distance, Angle. Spectral period d.c., spectral frequency 0.000 Hz, spectral amplitude 2.243 nm.

adsorbed material lowering the surface energy of the open crack as the microcracks propagate, in a manner analogous to that of hydrogen during the embrittlement of steel.

Atomic force microscopy (AFM) analysis of the etched chromium deposits provides further information about the third dimension of the SEM images as well as information about the width and depth of the microcracks. An AFM image is shown in Fig. 8. The microcracks developed by the caustic etch are seen throughout the chromium surface. Fine structure is also seen throughout the chromium deposit. The size of the microcracks varies within the deposit. A top view of Fig. 8 is seen in Fig. 9. Note the microcrack in the middle of the image appears larger than those transversing either the top or the bottom. Fine surface structure is also seen; these are the nodules often observed in chromium deposits and not the grains of chromium [13], Fig. 10. Sectional analysis of Figs 8 and 9 is seen in Fig. 11. Line traces across the microcrack shows the average depth of the etched microcrack is 268 mm. The widths of the microcracks vary from 0.3–0.91 μm and are of the same magnitude of the size of the microcracks from SEM analysis.

Inverting the AFM image of Fig. 8 shows the structure of the microcrack within the bulk of the chromium deposit, Figs 12 and 13. The base of the microcrack appears to exhibit a uniform structure and no points along the microcrack are significantly higher (or lower in the real image) than others. This indicates that microcracks penetrate only to a given

thickness, then the chromium coating starts to undergo microcracking somewhere else in the coating. If microcracking continued only in specific regions, the microcracks would traverse the length of the deposit as seen in cross-section, something that is not commonly observed in chromium plating. Sectional analysis of the inverted microcracks shows the average height (depth in the real image) is 267 nm and the width is of the order of 0.8 μm. The microcracks are thus approximately three times as wide as they are deep after etching.

4. Conclusions

The internal stress and subsequent microcracks in chromium electrodeposits was investigated. The stress decreases from a high initial value to a lower limiting stress owing to microcrack generation. Cracking occurs throughout the thickness of the deposit as is evident by subsurface microcracks detected in secondary electron SEM images. Etching the chromium deposits develops the microcrack patterns. *Y*-modulated images provide some insight into the third dimension of the microcracks and regions adjacent to the cracks. AFM analysis provides further information about the width and depth of the microcracks.

References

1. K. G. SODERBURG and A. K. GRAHAM, *Proc. Am. Electropl. Soc.* **34** (1947) 74.
2. A. W. HOTHERSALL and C. J. LEADBEATER, *J. Electrodep. Tech. Soc.* **14** (1938) 207.
3. H. FISHER, "Electrolytic Deposition and Electrocrystallization of Metals" (Springer, 1954).
4. R. WEIL, *AES Res. Project* **22** (1975).
5. F. H. REID, *Trans. Inst. Metal Finish.* **36** (1958) 74.
6. H. FISHER, P. HUHSE and F. PAWLEK, *Z. Metallkde* **47** (1956) 43.
7. H. BINDER and H. FISHER, *ibid.* **53** (1962) 161.
8. D. R. GABE and J. M. WEST, *Trans. Inst. Metal Finish.* **40** (1963) 1.
9. B. U. ADZIEV and Z. A. SOLOV'EVA, *Sov. Electrochem.* **15** (4) (1979) 386.
10. G. G. STONEY, *Proc. R. Soc.* **A82** (1909) 172.
11. R. H. D. BARKLIE and H. J. DAVIES, *Proc. Inst. Mech. Eng.* **731** (1930).
12. K. BAURMANN, N. QUAISER and M. ROCHNER, *Galvanotechnik*, **56** (1965) 2.
13. N. M. MARTYAK, PhD dissertation, Stevens Institute of Technology, Hoboken, NJ (1991).
14. R. DOW and J. E. STARECK, *Proc. Am. Electropl. Soc.* **40** (1953) 53.
15. J. E. STARECK, E. J. SEYB and A. C. TULUMELLO, *Plating* **41** (1954) 1171.
16. H. FRY, *Trans. Inst. Metal. Finish.* **32** (1955) 107.

Received 23 October 1995
and accepted 24 April 1996